Table 2 Transfusion history (n = 292)

Parameter	n (%)
Period of transfusion dependency, months	
≤12	87 (29.8)
13–30	106 (36.3)
≥31	92 (31.5)
Unknown	7 (2.4)
Total lifetime no. of RBC[1] units received	
≤40	62 (21.2)
41–160	132 (45.2)
≥161	87 (29.8)
Unknown	11 (3.8)
No. of RBC units[1] in the past year	
≤20	30 (10.3)
21–40	53 (18.2)
41–70	93 (31.8)
≥71	82 (28.1)
Unknown	34 (11.6)

[1] One RBC unit is made from 200 mL of whole blood.

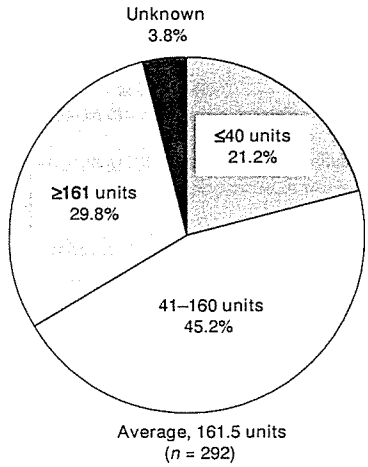

Figure 1 Transfusion history of patients: total lifetime red blood cell units.

32 months. Lifetime transfusions were: ≤40 units in 21.2%; >40–160 units in 45.2%; ≥161 units in 29.8%; and unknown in 3.8% of patients (Fig. 1). On average, patients received a total lifetime transfusions of 161.5 RBC units, and 61.5 RBC units in the year prior to data collection.

DFO chelation therapy

Less than half of the patients (126/292; 43.2%) had received DFO therapy, mostly on an intermittent basis; 164 of 292 patients (56.2%) were chelator-naïve and chelation history was unknown in two patients (0.7%). Among those who received DFO, 11 patients (8.6%) received daily/continuous DFO, with the remainder receiving intermittent DFO (mean; once/1.9 wk) or other regimens

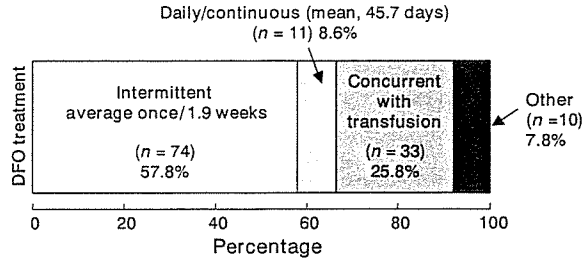

Figure 2 Proportion of patients receiving deferoxamine and regularity of treatment.

Table 3 Number of patients on various deferoxamine 500–1000 mg/d schedules

Route of administration	500 mg/d, n	1000 mg/d, n
Bolus intravenous	7	9
Subcutaneous	9	4
Intravenous (drip)	35	44
Intramuscular	9	0
Total	60	57

(Fig. 2). Intravenous drip infusion was the most common route of DFO administration, as shown in Table 3.

Of the DFO-treated patients, 53.7% had received ≤40 RBC units and 46.3% >40 units at the time of initiating DFO. On average, DFO was initiated in patients after receiving 61.6 RBC units. More than 95% of patients on DFO were monitored by serum ferritin, with 4.1% undergoing liver MRI.

Treatment with DFO was not associated with abnormality of total protein, SGOT, bilirubin, FBS, HbA_{1c}, and liver MRI scans or cause of death but was significantly associated with increased risk of abnormal SGPT ($P = 0.0072$), serum ferritin ≥1000 ng/mL ($P = 0.0385$), and cardiac dysfunction ($P = 0.0312$). Among patients with abnormal SGPT, serum ferritin, and cardiac dysfunction the majority received DFO. On the other hand, in patients receiving daily/continuously administered DFO serum ferritin, SGOT, SGPT, and FBS levels improved during treatment; pair-wise comparison using Wilcoxon two-sample test revealed that the proportion of patients with abnormal parameters in the daily/continuous DFO group was lower that on other DFO regimens (Table 4).

Assessment of serum ferritin

At the time of becoming TD, data on 142 patients revealed that the mean serum ferritin level was 1672.7 ng/mL and rose to 4378.3 ng/mL at EOS (n = 161; Fig. 3).

Serum ferritin levels were increased despite DFO usage. At the time of becoming TD and at EOS mean

Parameter	Intermittent (once/1.9 wk)	Concurrent with transfusion	Daily/continuous
Serum ferritin[1,2] (ng/mL)	+2222.8 (n = 36)	+2204.8 (n = 19)	−1135.2 (n = 9)
SGOT[1,3] (mU/mL)	+28.0 (n = 53)	+40.0 (n = 30)	−9.2 (n = 10)
SGPT (mU/mL)	+28.6 (n = 53)	+10.3 (n = 30)	−28.8 (n = 10)
FBS (mg/dL)	+31.2 (n = 31)	+8.2 (n = 12)	−4.8 (n = 5)

[1] Intermittent vs. continuous, $P < 0.05$.
[2] Continuous vs. concurrent, $P < 0.01$.
[3] Continuous vs. concurrent, $P < 0.05$.

Table 4 Average changes of laboratory values during the period of transfusion dependence in patients receiving deferoxamine treatment regimens

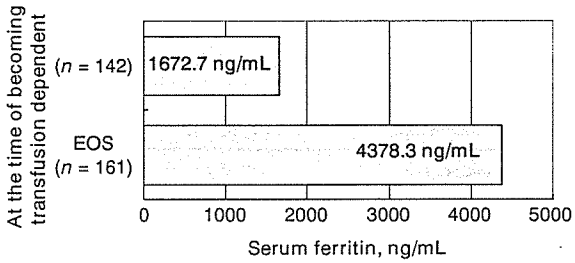

Figure 3 Serum ferritin levels at end of study and at the time of becoming transfusion-dependent.

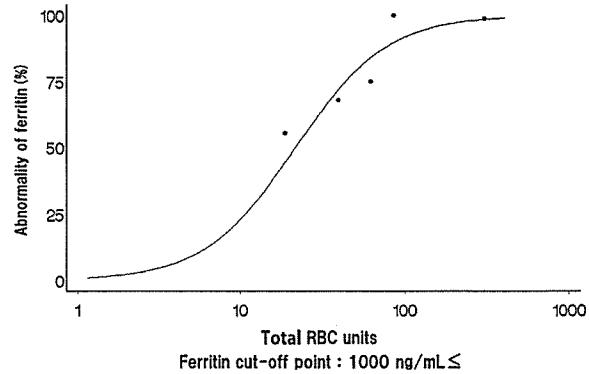

Figure 4 Relationship between end of study serum ferritin and total lifetime number of red blood cell units.

serum ferritin levels were 1590.1 and 4486.7 ng/mL, respectively, in patients who received DFO and 1465.8 and 3303.4 ng/mL, respectively, in chelator-naïve individuals. The proportion of patients with serum ferritin > 1000 ng/mL rose from 47.2% at the time of becoming TD to 89.4% at EOS.

Serum ferritin level was significantly correlated with lifetime total number of RBC units received ($P = 0.0072$) and number of RBC units received in the previous year ($P = 0.0004$) but was not correlated with age or underlying diseases. Figure 4 shows the relationship between the number of RBC units received and mean ferritin level, indicating the percentage of patients with an abnormal ferritin level (≥1000 ng/mL) for any total number of RBC units received as analyzed by logistics model. Patients were characterized by the number of RBC units, and the ratio to abnormal ferritin was categorized for each category. The goodness-of-fit of this model between theoretical and actual values was assessed by Pearson chi-squared test. The estimated number of RBC units required to raise ferritin to ≥1000 ng/mL in 50% and 75% of patients was calculated as 21.5 and 43.4 units, respectively.

There was a significant difference between the period of transfusion dependence in patients who received DFO and chelator-naïve patients (37.4 vs. 15.4 months; $P < 0.0001$). When comparing the monthly change of serum ferritin levels during the period of transfusion dependence between these two groups, DFO patients showed a slightly slower increase (77.9 vs. 162.3 ng/mL/month; $P = 0.0248$); this was nonetheless an abnormal increase. Among DFO-treated patients those who received daily/continuous DFO tended to show a slower increase in serum ferritin levels than those who received DFO by other schedules (45.8 vs. 78.5 ng/mL/month; $P = 0.6280$).

Laboratory values

The proportion of patients with abnormal laboratory parameters increased after initiation of transfusions: the proportion of patients in whom SGOT was ≥36 mU/mL [the upper limit of normal (ULN)] increased from 16.8% to 41.8%. Similarly, SGPT was ≥46 mU/mL (ULN) in 16.4% and 36.8% of patients before and after initiation of transfusions, respectively.

SGOT and SGPT abnormalities were significantly correlated with transfusion frequency ($P = 0.0016$ and < 0.0001, respectively), transfusion history ($P = 0.0099$ and 0.0009, respectively) and increased ferritin levels ($P = 0.0003$ and 0.0006, respectively) but not with age or underlying disease. There was a significantly ($P < 0.0001$) higher prevalence of SGOT (Fig. 5A) and SGPT (Fig. 5B) abnormality in patients with high serum ferritin than in those whose serum ferritin was < 1000 ng/mL. FBS was ≥121 mg/dL (ULN) in 39.1% and 54.0% of patients before and after initiation of transfusions, respectively. FBS abnormality was correlated with

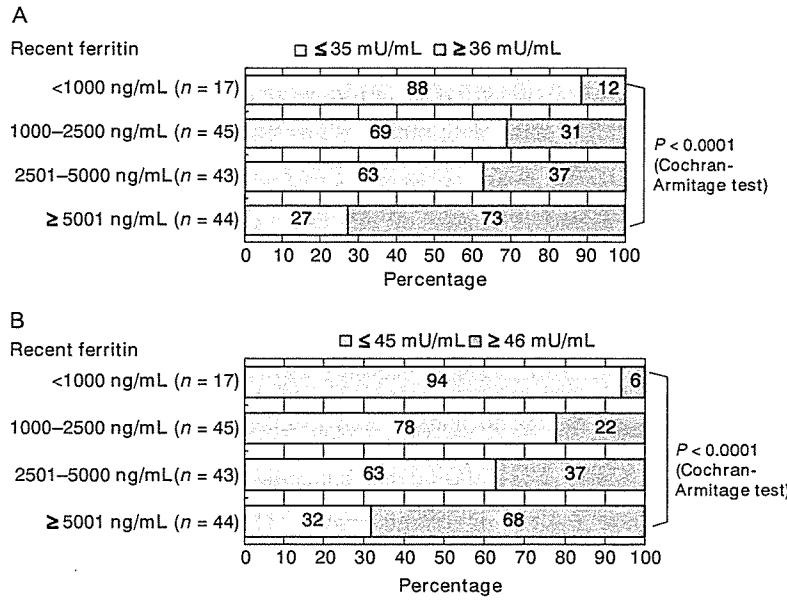

Figure 5 Relationship between serum glutamic oxaloacetic transaminase (A) and serum glutamic pyruvic transaminase (B) abnormality and serum ferritin.

Table 5 Sensitivity and specificity of serum ferritin levels ≥1000 and ≥2500 ng/mL to predict for abnormal SGOT/SGPT and cardiac function

	Serum ferritin (1000 ng/mL)		Serum ferritin (2500 ng/mL)	
Abnormality	Sensitivity	Specificity	Sensitivity	Specificity
SGOT	0.97	0.18	0.75	0.54
SGPT	0.98	0.17	0.55	0.81
Cardiac function	0.92	0.06	0.67	0.36

SGOT, serum glutamic oxaloacetic transaminase; SGPT, serum glutamic pyruvic transaminase.

transfusion frequency ($P = 0.0072$) but not with transfusion history, serum ferritin, age, or underlying disease.

Among patients with abnormal laboratory parameters >90% had serum ferritin levels >1000 ng/mL. Serum ferritin was calculated a predictor of abnormality of EOS SGOT, SGPT, and cardiac function with sensitivities and specificities as shown in Table 5.

Assessment of organ function and cause of death

Of patients in whom cardiac function and liver MRI were evaluated, abnormalities were observed in 21.9% (14/64) and 84.6% (11/13), respectively. Among patients with cardiac dysfunction and those who underwent liver MRI, 91.7% (11/12) and 91.9% (10/11), respectively, had serum ferritin levels ≥1000 ng/mL. Cardiac abnormality was weakly correlated with serum ferritin levels. Patients with cardiac abnormality showed greater increases of serum ferritin levels than those who did not (7096.0 vs. 4220.1 ng/mL; $P = 0.0392$). There was no correlation observed between MRI abnormality and patient background or transfusion history.

In total, 75 deaths were reported. Most of the deaths were caused by infection and leukemia; however, cardiac and liver failure was noted in 24.0% and 6.7% of cases, respectively. There was a significant difference between the number of patients who died from leukemia or infection and those whose cause of death was reported as cardiac/liver failure in terms of transfusion history.

There was no significant difference in mean age between patients who died from iron overload (cardiac or liver failure) and those who died from other causes ($P = 0.6767$; Fisher test). Among patients with MDS, 11 died of cardiac or liver failure. Of these, 10 patients (90.9%) were classified as International Prognostic Scoring System low/intermediate-1 risk whereas one patient (9.1%) was intermediate-2/high risk. Sixty-four percent of the patients with MDS who died became TD when aged 50–60 yr, and the mean duration from onset of transfusion dependence to death was 30.5 months.

Patients who died from cardiac or liver failure had more transfusions than those who died from other causes (total RBC units = 289.2 vs. 160.7 units, respectively; $P = 0.0033$). Furthermore, among 38 patients in whom serum ferritin levels were available, almost all ($n = 37$) died with serum ferritin levels ≥1000 ng/mL, whereas only one patient had a serum ferritin level <1000 ng/mL. Twenty four of these patients had serum ferritin levels >5000 ng/mL.

Discussion

This was the first nationwide survey to investigate morbidity/mortality resulting from iron overload in Japanese TD patients with refractory anemias. A high serum

ferritin level was correlated with cardiac and liver dysfunction, and more patients died with serum ferritin levels ≥1000 ng/mL than < 1000 ng/mL. Further observations may clarify the effect of history of transfusions on death. The compelling results of this study suggest that a randomized study comparing effective chelation therapy vs. no treatment would not be ethical. However, a prospective survey of effectively chelated patients, in comparison with the results of this retrospective study, would be of great value to physicians in underlining the devastating impact of iron overload in patients with TD anemias. Overall, the results presented here seem useful for establishing guidelines for the treatment of iron-overloaded patients with MDS and AA in Japan, indicating the need to address iron overload in these patient populations (11–14).

Cause of death was reported as cardiac failure in 24% and liver failure in 6.7% of patients studied. Therefore multiple transfusion therapy for anemias such as MDS and AA was confirmed associated with a high risk for developing fatal comorbidities caused by chronic iron overload. This result is in line with a recent report showing that TD MDS patients exhibited a significantly shorter overall survival than MDS patients who did not require transfusions, and that developing secondary iron overload significantly affected survival (15).

Cardiac examination was conducted in only 64 cases (21.9%); however, among these cases 14 patients (21.9%) showed signs of cardiac abnormality. Cardiac risk was weakly correlated with the presence/absence of DFO therapy, with DFO-treated patients exhibiting a slightly higher risk of cardiac dysfunction. It is not certain as to how far this result reflects the clinical tendency for patients with cardiac dysfunction to be selected as candidates for treatment with DFO. Although DFO is cardioprotective in TD patients (16, 17), the effects of DFO on reversing congestive heart failure could not be assessed in the present series. We recommend that cardiac function be carefully monitored, and the effect of iron overload on the heart examined in detail.

The pathological effects of transfusional iron overload on liver and pancreas are well documented, and major iron deposition in these organs usually precedes that in cardiac myocytes (18). Hemosiderin in pancreatic islet cells has been shown to increase with the number of blood transfusions in iron-overloaded patients with a history of glycosuria and hyperglycemia. Furthermore, in comparison with normal controls, increased glucose intolerance associated with significantly reduced insulin output was observed in non-thalassemic patients with anemias requiring transfusions (18, 19). In the present study of TD patients SGOT, SGPT, and FBS were time-dependently increased from the time of becoming TD. No such effect was observed on total protein, bilirubin, and HbA_{1C}. Abnormality of serum liver enzymes was significantly correlated with history of transfusion and serum ferritin levels but not with age and underlying disease; FBS was also correlated with frequency of transfusion. These observations confirm previous reports that liver and pancreatic dysfunction occur as a result of iron overload from repeated transfusions.

Ferritin tests were conducted in 50–70% of patients. This procedure was very common and seems more practical for monitoring patients than liver MRI and biopsy. Serum ferritin was significantly correlated with frequency and history of transfusion, and appears useful for monitoring iron overload. Ferritin was also well correlated with SGOT/SGPT and cardiac dysfunction. Patients with high serum ferritin levels ≥1000 ng/mL had an increased risk of liver enzyme abnormality as well as increased risk of cardiac dysfunction and death caused by iron overload. Hence serum ferritin is a useful marker to predict clinical comorbidity resulting from iron overload.

The number of RBC units required to raise serum ferritin levels to ≥1000 ng/mL in 50% and 75% of patients was 21.5 and 43.4 units, respectively. Therefore from these data it is reasonable to consider that iron chelation therapy should start when serum ferritin reaches 1000 ng/mL or after transfusion of 20–40 units of total RBC units so as to avoid the risk of end-organ damage caused by toxic free iron. Indeed, it is recommended in various guidelines that serum ferritin levels be maintained < 1000 ng/mL by iron chelation therapy (12, 14, 20, 21).

In the patients assessed in this study the sensitivity and specificity of EOS serum ferritin levels were calculated and correlated with abnormal EOS SGOT, SGPT, and cardiac function. These results show that serum ferritin level is a highly sensitive and useful indicator for monitoring chelation therapy, and strongly suggest that effective chelation therapy with a long period of chelation coverage should be administered to prevent cardiac as well as other organ dysfunction.

It is widely acknowledged that continuous exposure to DFO provides optimal efficacy (14). In the treatment of thalassemia full compliance or increasing the overall period of chelation coverage (> 300 d/yr) is strongly correlated to length of survival (22). However, in our series DFO was mostly given intermittently (once/1.9 wk) or administered concurrently with transfusion. It is difficult to administer DFO daily/continuously especially in MDS and AA patients who may be at risk of infection or bleeding because of peripheral cytopenia. Furthermore, most patients in Japan receive treatment on an outpatient basis, and infusion pumps for DFO therapy are not reimbursed.

DFO-treated patients showed a slightly lower monthly increase in serum ferritin levels during the period of

transfusion dependence than chelator-naïve patients but this was nonetheless abnormally increased. DFO suppressive efficacy was not seen in laboratory values, cardiac/liver function, or death from iron overload. Taken together, these results imply that the current treatment methodology in Japan (often once/2 wk) might not be clinically the most effective. Patients who received daily/continuous (average, 45.7 d) DFO treatment, on the other hand, exhibited decreases in serum ferritin levels; SGOT, SGPT, and FBS and were less likely to display abnormal laboratory values.

Daily DFO treatment (5–7 d/wk) is the reference standard of care for patients with β-thalassemia, and effective DFO therapy has been clearly demonstrated to prolong survival in thalassemic patients as well as those with MDS (23, 24). Furthermore, daily DFO treatment elicits prophylactic effects against cardiac dysfunction and diabetes (25). In a small trial conducted in 11 patients with MDS daily/continuous DFO chelation improved serum ferritin and hemoglobin requirement of the patients (26).

The only other approved chelators are for use as second-line treatment for β-thalassemia. Recently, a novel oral iron chelator, deferasirox, has been approved in >60 countries. Deferasirox is easily absorbed and has a median elimination half-life of 8–16 h, which means that deferasirox is continuously present in the plasma with once-daily dosage (27). In a large phase III trial deferasirox was comparable with DFO at decreasing iron burden in β-thalassemic patients with a liver iron concentration >7 mg Fe/g dry weight (28). Deferasirox also reduced iron burden in patients with various anemias including MDS (29). These findings indicate that the availability of oral iron chelators, especially deferasirox, can improve patients' QoL by ameliorating organ dysfunction and preventing iron damage. This may ultimately prolong survival of patients receiving treatment with an oral iron chelator.

Conclusions

This retrospective analysis of TD patients with anemias such as MDS and AA revealed that the mortality rate is raised in heavily iron-overloaded patients, with liver and cardiac dysfunction being the primary cause of death. Serum ferritin level appears a useful monitor of iron overload. Daily/continuous chelation therapy was effective in reducing iron burden and improving organ function; however, practical implementation of continuous administration is currently difficult. Based on these findings chelation therapy should be initiated at a serum ferritin level of ≥1000 ng/mL, using a regimen that provides the longest possible period of chelation coverage with the least intrusion on patient QoL.

Acknowledgement

This work was supported in part by a grant from the Ministry of Health, Welfare, and Labor of Japan (Research on Measures for Intractable Diseases).

References

1. Japan Intractable Diseases Information Center. Available at: http://www.nanbyou.or.jp.
2. Gabutti V, Borgna-Pignatti C. Clinical manifestations and therapy of transfusional haemosiderosis. *Bailliere's Clin Haematol* 1994;**7**:919–40.
3. McLaren GD, Muir WA, Kellermeyer RW. Iron overload disorders: natural history, pathogenesis, diagnosis, and therapy. *Crit Rev Clin Lab Sci* 1983;**19**:205–66.
4. Kushner JP, Porter JP, Olivieri NF. Secondary iron overload. In: *Hematology/American Society of Hematology Education Program Book*. American Society of Hematology, 2001. Available at: http://www.asheducationbook.org/cgi/content/full/2001/1/47.
5. Ehlers KH, Levin AR, Markenson AL, Marcus JR, Klein AA, Hilgartner MW, Engle MA. Longitudinal study of cardiac function in thalassemia major. *Ann New York Acad Sci* 1980;**344**:397–404.
6. Bassett ML, Halliday JW, Powell LW. Value of hepatic iron measurements in early hemochromatosis and determination of the critical iron level associated with fibrosis. *Hepatology* 1986;**6**:24–29.
7. Adams PC, Deugnier Y, Moirand R, Brissot P. The relationship between iron overload, clinical symptoms, and age in 410 patients with genetic hemochromatosis. *Hepatology* 1997;**25**:162–6.
8. De Sanctis V, Zurlo MG, Senesi E, Boffa C, Cavallo L, Di Gregorio F. Insulin dependent diabetes in thalassaemia. *Arch Dis Child* 1988;**63**:58–62.
9. Weiss G. Iron and immunity: a double-edged sword. *Eur J Clin Invest* 2002;**32**(s1):70–78.
10. Bullen JJ. The significance of iron in infection. *Rev Infect Dis* 1981;**3**:1127–38.
11. Greenberg PL, Baer MR, Bennett JM, *et al.* Myelodysplastic syndromes: clinical practice guidelines in oncology. *J Natl Comp Cancer Net* 2006;**4**:58–77.
12. Bowen D, Culligan D, Jowitt S, Kelsey S, Mufti G, Oscier D, Parker J. Guidelines for the diagnosis and therapy of adult myelodysplastic syndromes. *Br J Haematol* 2003;**120**:187–200.
13. Alessandrino EP, Amadori S, Barosi G, *et al.* Evidence- and consensus-based practice guidelines for the therapy of primary myelodysplastic syndromes. A statement from the Italian Society of Hematology. *Haematologica* 2002;**7**:1286–306.
14. Gattermann N, Porter J, Lopes LF, Seymour J. Consensus statement on iron overload in myelodysplastic syndromes. *Hematol Oncol Clin North Am* 2005;**19**(s1):18–25.

15. Malcovati L, Della Porta MG, Pascutto C, *et al.* Prognostic factors and life expectancy in myelodysplastic syndromes classified according to WHO criteria: a basis for clinical decision-making. *J Clin Oncol* 2005;**23**:7594–603.
16. Wolfe L, Olivieri N, Sallan D. Prevention of cardiac disease by subcutaneous deferoxamine in patients with thalassemia major. *N Engl J Med* 1985;**312**:1600–3.
17. Giardina PJ, Ehlers KH, Engle MA, Grady RW, Hilgartner MW. The effect of subcutaneous deferoxamine on the cardiac profile of thalassemia major: a five-year study. *Ann New York Acad Sci* 1985;**445**:282–92.
18. Schafer AI, Cheron RG, Dluhy R. Clinical consequences of acquired transfusional iron overload in adults. *N Engl J Med* 1981;**304**:319–24.
19. Lu J-P, Hayashi K. Selective iron deposition in pancreatic islet B cells of transfusional iron-overloaded autopsy cases. *Pathol Int* 1994;**44**:194–9.
20. Thalassaemia International Federation. *Guidelines for the Clinical Management of Thalassaemia*. Thalassaemia International Federation, 2002. Available at: http://www.thalassaemia.org.cy/Publications.htm.
21. National Comprehensive Cancer Network. *Clinical Practice Guidelines in Oncology*. Myelodysplastic Syndromes-v.4. 2006. NCCN, 2006. Available at: http://www.nccn.org.
22. Modell B, Khan M, Darlison M. Survival in beta-thalassaemia major in the UK: data from the UK Thalassaemia Register. *Lancet* 2000;**355**:2051–2.
23. Leitch HA, Goodman TA, Wong KK, Vickars LM, Galbraith PF, Leger CS. Improved survival in patients with myelodysplastic syndrome (MDS) receiving iron chelation therapy. *Blood* 2006;**108**:abstract 249.
24. Gabutti V, Piga A. Results of long-term iron-chelating therapy. *Acta Haematol* 1996;**95**:26–36.
25. Brittenham GM, Griffith PM, Nienhuis AW, McLaren CE, Young NS, Tucker EE, Allen CJ, Farrell DE, Harris JW. Efficacy of deferoxamine in preventing complications of iron overload in patients with thalassemia major. *N Engl J Med* 1994;**331**:567–73.
26. Jensen PD, Heickendorff L, Pedersen B, Bendix-Hansen K, Jensen FT, Christensen T, Boesen AM, Ellegaard J. The effect of iron chelation on haemopoiesis in MDS patients with transfusional iron overload. *Br J Haematol* 1996;**94**:288–99.
27. Piga A, Galanello R, Forni GL, *et al.* Randomized phase II trial of deferasirox (Exjade, ICL670), a once-daily, orally-administered iron chelator, in comparison to deferoxamine in thalassemia patients with transfusional iron overload. *Haematologica* 2006;**91**:873–80.
28. Cappellini MD, Cohen A, Piga A, *et al.* A phase 3 study of deferasirox (ICL670), a once-daily oral iron chelator, in patients with beta-thalassemia. *Blood* 2006;**107**:3455–62.
29. Porter J, Vichinsky E, Rose C, Piga A, Olivieri N, Gattermann N, Maertens J, Rabault B, Gathmann I, Alberti D. A phase II study with ICL670 (Exjade®), a once-daily oral iron chelator, in patients with various transfusion-dependent anemias and iron overload. *Blood* 2004;**104**:abstract 3193.

International Society for Cellular Therapy ISCT

Cytotherapy (2007) Vol. 9, No. 1, 80–90

informa healthcare

Screening of genes responsible for differentiation of mouse mesenchymal stromal cells by DNA micro-array analysis of C3H10T1/2 and C3H10T1/2-derived cell lines

I Oh[1], K Ozaki[1], A Miyazato[1], K Sato[1], A Meguro[1], K Muroi[3], T Nagai[1], H Mano[2] and K Ozawa[1]

[1]*Division of Hematology, Department of Medicine*

[2]*Division of Functional Genomics, Center for Molecular Medicine*

[3]*Division of Cell Transplantation and Transfusion, Jichi Medical University, Tochigi, Japan*

Background

The molecular mechanisms underlying the biologic effects or differentiation of mesenchymal stromal cells (MSC) have not been clarified. Screening for genes differentially expressed at different stages is an important step in determining these molecular mechanisms.

Methods

In this study, we analyzed the gene expression profiles of C3H10T1/2 (10T1/2) cells and two sublines, A54 (pre-adipocyte) and M1601 (myoblast), as a model of MSC and downstream committed progenitors.

Results

We found up-regulated expression of delta-like-1 (Dlk), Wnt-5a and IL-1 receptor-like-1 (ST2) in 10T1/2 cells; stem cell factor (SCF) and stromal derived factor-1 (SDF-1) in A54 cells; and cardiac muscle-specific gene in M1601 cells. Overexpression of Dlk in A54 cells did not induce any effects on their differentiation into adipocytes. After differentiation into adipocytes, A54 cells reduced the expression of SCF, SDF-1 and Ang-1 as well as the ability to support the formation of a cobblestone appearance.

Discussion

The results suggest that these three lines have different gene profiles and are a useful system for analyzing the differentiation and function of MSC and progenitor cells.

Keywords

mesenchymal stromal cells, 10T1/2, DNA micro-array, expression profiles.

Introduction

Mesenchymal stromal cells (MSC) are a non-hematopoietic component of BM. These cells account for a small portion of BM and they have the capacity to differentiate into adipocytes, osteocytes and chondrocytes [1]. Because MSC can be readily isolated and expanded *in vitro*, it is expected that they can be used for regenerative therapies. Recent studies have demonstrated that MSC are capable of supporting hematopoiesis and regulating the immune response [2–5]. Clinical studies have been carried out regarding the use of MSC for suppressing GvHD in allogeneic stem cell transplantation [6,7] and for regenerative therapy [8,9]; however, the molecular mechanism underlying the biologic effects of MSC remains unclear. The identification of key molecules for the differentiation, immunosuppression and hematopoietic support of MSC is a crucial step for their clinical application.

Some investigators have used the 10T1/2 cell line, derived from C3H mouse embryo cells, as a model of mouse MSC [5,10]. In the presence of 5-azacytidine, 10T1/2 cells can be differentiated into adipocytes, osteocytes and chondrocytes [11]. We have previously

Correspondence to: Katsutoshi Ozaki, MD, PhD, and Keiya Ozawa, MD, PhD, Division of Hematology, Jichi Medical University, Tochigi 329-0498, Japan. E-mail: ozakikat@jichi.ac.jp; kozawa@ms2.jichi.ac.jp.

DOI: 10.1080/14653240601016374

established two sublines from 10T1/2, designated A54 (pre-adipocyte) and M1601 (myoblast) [12]. Under appropriate conditions, A54 and M1601 cells can terminally differentiate into adipocytes and myotubes, respectively, whereas the parental 10T1/2 cells remain undifferentiated under the same conditions [12].

Ang-1 is expressed on osteoblasts in the BM niche, and Tie-2, the receptor for Ang-1, is expressed on vascular endothelium and hematopoietic stem cells [13]. It has been suggested that the interaction between Ang-1 and Tie-2 is essential for cobblestone formation by hematopoietic stem cells *in vitro* [14]. Activation of Tie-2 is reported to participate in the self-renewal of hematopoietic stem cells within the BM niche [14]. Except for its expression in osteoblasts, the distribution of Ang-1 expression in the BM has not been clearly determined.

In the present study, we used 10T1/2 cells as a model of MSC and A54 and M1601 cells as committed mesenchymal progenitors, and compared their gene expression profiles by DNA micro-array analysis. We found that each cell line showed unique gene expression profiles. Furthermore, we identified several molecules that might participate in the differentiation of MSC.

Methods

Cell lines and induction of terminal differentiation

The parental 10T1/2 cell line was obtained from the Japanese Cancer Research Resources Bank (Tsukuba, Japan) and the two derivative cell lines, A54 and M1601, were established as described previously [12]. All cell lines were cultured in Iscove's modified Dulbecco's medium (Invitrogen, Carlsbad, CA, USA) supplemented with 10% FCS (Sigma, St Louis, MO, USA). Adipocyte differentiation of A54 cells was induced by incubating them for 7 days in medium supplemented with 10^{-5} M insulin (Sigma) and 10^{-6} M dexamethasone (Wako, Osaka, Japan). Myotube differentiation of M1601 cells was induced by incubating them for 7 days in medium containing 2% horse serum (GIBCO, Gland Island, NY, USA) instead of FCS.

Oligonucleotide micro-array

Total RNA was extracted from the cells using RNeasy (QIAGEN, Valencia, CA, USA) and 10 μg total RNA was subjected to cDNA synthesis using a T7-$(dT)_{24}$ primer that contained the T7 promoter sequence. After second-strand synthesis, *in vitro* transcription was performed to synthesize biotin-labeled complementary RNA (cRNA). The cRNA (15 μg) was hybridized for 16 h at 45°C onto an Affymetrix Mouse Genome U74A version-2 GeneChip (Affymetrix, CA, USA), which contains more than 6000 target genes. The hybridized chip was washed and stained with streptavidin-conjugated PE using the fluidics station. The fluorescence signal intensity was captured by a laser scanner and calculated using Microarray Suite version 5.0 (Affymetrix).

Micro-array data analysis

GeneSpring software (Silicon Genetics, Foster, CA, USA) was used for the analysis of micro-array data. To eliminate noise, only transcripts with more than a 2-fold increase in relative intensity and those indicated as 'present' by Microarray Suite version 5.0 (Affymetrix) were selected as up-regulated genes.

Quantitative real-time RT-PCR

Total RNA was extracted from the cells and cDNA was synthesized using the SuperScript® first-strand synthesis kit (Invitrogen) from 4 μg total RNA. PCR was performed with 1/30th of the original cDNA synthesis reaction (corresponding to 133 ng total RNA) using a Quantitect® SYBR Green PCR kit (QIAGEN) according to the manufacturer's instructions. The incorporation of the SYBR green dye into the PCR products was monitored with an ABI Prism 7700 sequence detection system (PE Applied Biosystems, Foster, CA, USA). A standard curve was produced in each reaction to confirm the target product was within the standard curve and to calculate the copy number of the target. To create templates for the standard curve, PCR products were directly cloned into a plasmid vector (TOPO TA Cloning® Kits for sequencing; Invitrogen). After determination of the plasmid DNA concentration, the copy number of the standard could be calculated using the following formula: DNA concentration /(plasmid length in base pairs $\times$ 660) $\times$ 6.022×10^{23}.

Quantitative RT-PCR was repeated three times using the same cDNA but at different time points. Statistical analysis was based on the Student's t-test. $P < 0.05$ was considered statistically significant.

Flow cytometric analysis

PE-conjugated rat anti-mouse CD90.2 MAb was from BD Pharmingen (San Diego, CA, USA). Rat anti-mouse Dlk

mAb was a gift from Dr Atsushi Miyajima (University of Tokyo, Tokyo, Japan). PE-conjugated goat anti-rat IgG was from Cederlane (Ontario, Canada). Fc block (BD Pharmingen) was used to prevent non-specific binding of Ab to Fc receptors. Cells were stained with MAb for 30 min on ice. Flow cytometric analysis was performed using a BD LSR (Becton Dickinson, San Diego, CA, USA) and the collected data were analyzed using CELLQUEST software (Becton Dickinson).

Retrovirus-mediated gene transduction

A54 cells were infected with either empty MSCV-IRES-EGFP retroviral vectors or the one encoding hDlk (MSCV-IRES-EGFP vector was a gift from Dr Akihiro Kume, Jichi Medical School, Tochigi, Japan) [15]. Retroviral vectors were transiently transfected into the BOSC23 packaging cell line using Lipofectamine® and Plus reagent (Invitrogen). Supernatants from BOSC23 were supplemented with 4 μg/mL polybrene. Transduction into A54 cells was accomplished by centrifugation at 1080 *g* for 40 min at 32°C, followed by incubation for 4 h at 37°C.

Co-culture of the mouse hematopoietic stem cell fraction with 10T1/2, A54 and M1601 cells

BM cells were obtained from the femurs of 10-week-old C3H/HeN mice by flushing with PBS (Invitrogen). BM suspensions were layered over 1.087 g/mL Lympholyte-M (Cedarlane, Ontario, Canada) and centrifuged at 480 *g* for 30 min to obtain BM mononuclear cells. These cells were magnetically labeled with a cocktail of biotinylated Ab to lineage markers, including CD5, B220, CD11b, Gr-1, 7-4 and Ter119, followed by anti-biotin microbeads (Miltenyi Biotec, Auburn, CA, USA). Magnetically labeled cells were depleted with AutoMACS (Miltenyi Biotec) according to the manufacturer's instructions. Subsequently, the lineage-negative fraction was magnetically labeled with anti-Sca-1 microbeads (Miltenyi Biotec) and positively selected. Lin(−)Sca-1(+) cells (2.4×10^4) were plated on 2×10^4 10T1/2, A54 or M1601 cells in 12-well dishes and co-cultured for 6 days. Prior to co-cultivation, the 10T1/2, A54 and M1601 cells were irradiated with 30 Gy to prevent excess proliferation. Hematopoietic cobblestone formation was evaluated by phase-contrast microscopy.

Western blot analysis

Protein samples were extracted from 10T1/2, A54, M1601 and OP9 cells using an NP-40-based cell lysis buffer. Equal amounts of protein (20 μg) were fractionated by SDS–PAGE. The proteins were then electrophoretically transferred onto PVDF membranes (Invitrogen) and blotted with an Ab to mouse Ang-1 (1:10000; Santa Cruz Biotechnology, Santa Cruz, CA, USA) or a MAb to β-actin (1:5000; Sigma), followed by horseradish peroxidase-conjugated anti-mouse or anti-rabbit Ig Ab (Amersham Biosciences, Uppsala, Sweden). Blots were visualized using West Pico chemiluminescent reagent (Pierce, Rockford, IL, USA) and exposure to X-ray film (Kodak, Rochester, NY, USA).

Results

Terminal differentiation of 10T1/2-derived cells into adipocytes or myotubes

Previously we had established two sublines, pre-adipocyte A54 and myoblast M1601 cells, from the parental mouse embryo fibroblast cell line 10T1/2 by treatment with 5-azacytidine [12]. 10T1/2, A54 and M1601 exhibit similar morphologies under maintenance conditions. A54 and M1601 cells can be differentiated into adipocytes and myotubes, respectively, under appropriate conditions,

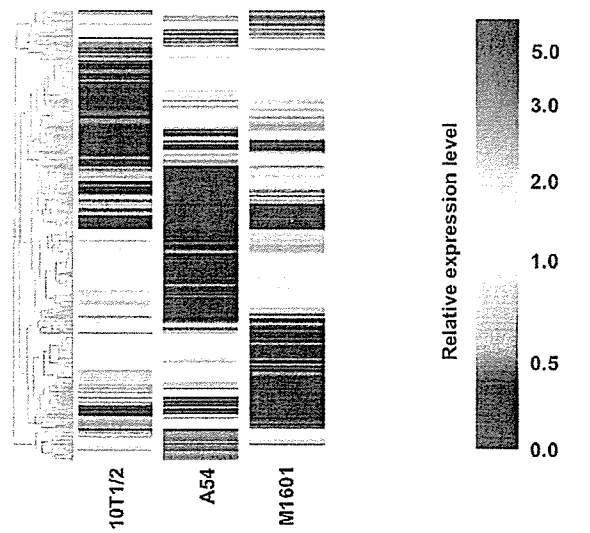

Figure 1. Gene expression profiles of 10T1/2, A54 and M1601 cell lines. Hierarchical clustering analysis of selected genes based on their expression patterns in 10T1/2 and 10T1/2-derived cell lines was performed, and the results are shown as a dendrogram. The relative signal intensity was calculated and color-coded as indicated on the right. Each row corresponds to a single gene.

Table 1. Genes up-regulated in 10T1/2 (A), A54 (B) and M1601 (C) Genes specifically up-regulated in 10T1/2, A54 and M1601 cells are listed. Functionally unknown genes have been excluded to simplify the lists. The common name.

A

Genbank ID	Common name	Description
U69137	Cdh10	cadherin 10
AF100778	Wisp2	WNT inducible signaling pathway protein 2
AW120746	Scoc	short coiled coil proten
AI845934	Ebna1bp2	EBNA1 binding protein 2
AI854020	Cd01	cysteine dioxygenase 1. cytosolic
AF059567	Cdkn2b	cylin-dependent kinase inhibitor 2B (p 15. inhibits CDK4)
X69619	Activin	inhibin beta-A
Y09257	nov	nephroblastoma overexpressed gene
Z12171	dlk	delta-like 1 homolog (Drosophila)
AF002718	IF1	ATPase inhibitor
AI839950	Fhl11	four and a half LIM domains 1
AB017697	TLP21	TATA box binding protein-like 1
AI849615	Gas5	growth arreset specific 5
AI853375	Mdm2	transformed mouse 3T3 cell double minute 2
AB021228	mt3-mmp	matrix metalloproteinase 16
D13695	ST2	interleukin 1 receptor-like 1
M28845	Krox-24	early grown response 1
X90875	FXR1	fragile X mental retardation gene 1. autosomal homolog
X90875	Wnt-5a	wingless-related MMTV integration site 5A
M89798	NCX1	solute carrier family 8 (sodium/calcium exchanger). member 1
AF004666	Cdkn2a	cyclin-dependent kinase inhibitor 2A
AF044336	Thy-1.2 (CD90.2)	thymus cell antigen 1. theta
X60367	CRBPI	Retinol binding protein 1, cellular
AF022072	Grb10	Growth factor receptor bound protein 10

B

Genbank ID	Common name	Description
U49513	Cc19	chemokine (C-C motif) ligand 9
X61800	C/ebp delta	CCAAT/enhancer binding protein (C/EBP), delta
J04596	Cxcl1	chemokine (C-X-C motif) ligand 1
X70058	CCL7;MCP-3	chemokine (C-C motif) ligand 7
M62362	mc/EBP	Mouse CAATT/enhancer binding protein gene
AF002719	SLPI	secretory leukocyte protease inhibitor
X79199	Tna	tetranectin (plasminogen binding protein
AV139913	Cxcl12	chemokine (C-X-C motif ligand 12
AF004874	Ltbp2	latent transforming growth factor beta binding protein 2
X56848	BMP-4	bone morphogenetic protein 4
AF054623	frizzled-1	frizzled homolog 1, (Drosophila)
X57413	TGF-beta2	transforming growth factor, beta 2
U27267	Cxcl5	chemokine (C-X-C motif) ligand 5
U88566	Sfrp1	secreted frizzled-related sequence protein 1
M62362	mc/EPB	CCAAT/enhancer binding protein (C/EBP), alpha
X83202	11beta-HSD1A	hydroxysteroid 11-beta dehydrogenase 1
AF011450	Col15a1	procollagen, type XV
M57647	SCF	kit ligand
U49915	adipoQ	adipocyte complement related protein
U10374	Pparg	Peroxisome proliferators-activated receptor gamma
X04480	Igf1	insulin-like growth factor 1
X66405	Col6a1	procollagen, type VI, alpha 1

Table 1 (*Continued*)

L19932	beta ig-h3	transforming growth factor, beta induced 68 kDa
U60091	TAP2-cas	transporter 2, ATP-binding cassette, sub-family B (MDR/TAP)

C

Genbank ID	Common name	Description
U21301	Mertk	c-mer proto-oncogene tyrosine kinase
L48989	Tnnt3	troponin T3, sakeletal, fast
U77943	Mylpf; Mlc2; MLC-2	myosin light chain
M25944	Car2; Call; Car-2:	carbonic anhydrase 2
M14537	Chrnb1	cholinergic receptor, nicotinic, beta polypeptide 1
Z38015	DM-PK	dystrophia myotonica kinase, B15
AF000236	Cmkor1	chemokine orphan receptor 1
AV362816	Star	steroidogenic acute regulatory protein
AV324706	Ncam1	neural cell adhesion molecule 1
AV248455	Chrng	cholinergic receptor, nicotnic, gamma polypeptide
M74753	Myh3	myosin, heavy polypeptide 3
M18879	MyoD	myogenic differentiation 1
X12973	Mylf; MLC1f; MLC3f	myosin light chain, alkali, fast skeletal muscle
D26532	Runx1	runt related transcription factor 1
X67140	Atp2a1	ATPase, Ca+ + transporting
U73620	Vegfc; VEGF-C	vascular endothelial growth factor C
D88689	Flt 1	FMS-like tyurosine kinase 1
AF041847	Crap; Alrp; CARP	cardiac responsive adriamycin protein
AFO42487	Kcnn4	potassium conductance calcium-activated channel
AF045801	Cktsf1b1	cysteine knot superfamily 1, BMP antagonist 1
M12347	alpha-actin	actin, alpha 1, skeletal muscle
Z80112	Icr-1	chemokine (C-X-C motif) receptor 4

whereas parental 10T1/2 cells maintain the same morphologic phenotype under the same conditions (see the Methods) [12].

Gene expression profiles of 10T1/2 and 10T1/2-derived cells

Using these three cell lines as a model of MSC and downstream progenitors, we performed high-throughput gene analysis to identify genes important for the differentiation of MSC. Total RNA from these three cell lines was subjected to biotinylation and hybridization with an Affymetrix GeneChip containing more than 6000 genes. Gene transcripts showing a more than 2-fold increase in relative intensity compared with the other two cell lines were selected. Each of the three cell lines (10T1/2, A54 and M1601) showed a unique gene expression profile despite morphologic similarities (Figure 1).

We identified 105 genes that were elevated in the parental 10T1/2 cells, including *activine*, *Dlk*, *Nov*, *Grb10*, *p15* and many functionally uncharacterized molecules (Table 1A). *Dlk* and *Nov* are known to be involved in the Notch signaling pathway and are reported to have the ability to inhibit MSC differentiation into adipocytes and osteoblasts [16,17]. In pre-adipocyte A54 cells, we found 201 genes that were up-regulated. These included genes known to be involved in adipocyte differentiation, such as *C/EBPα*, *C/EBPδ*, *PPAR-γ*, *PAI-I* and *Frizzled-1* (Table 1B) [18–21]. Finally, the myoblast M1601 cells showed 137 up-regulated genes, including ones related to skeletal muscle differentiation, such as *MyoD*, *MLC1F*, *α-skeletal actin*, *myosin heavy chain* and *myosin light chain* [22], as well as genes related to cardiac muscle differentiation, including *α-cardiac actin*, *cardiac troponin C* and *troponin T2* (Table 1C) [23].

Real-time PCR analysis of selected genes from micro-array experiments in parental 10T1/2 cells

Next, we selected six genes, *Dlk*, *Wnt-5a*, *ST2*, *CrbpI*, *p15* and *CD90*, as candidates for further analysis in 10T1/2 cells. According to the micro-array data, these genes had a more than 3-fold higher expression in 10T1/2 than in the other two cell lines. To confirm this differential expression, we performed RT real-time PCR. As shown in Figure 2A,

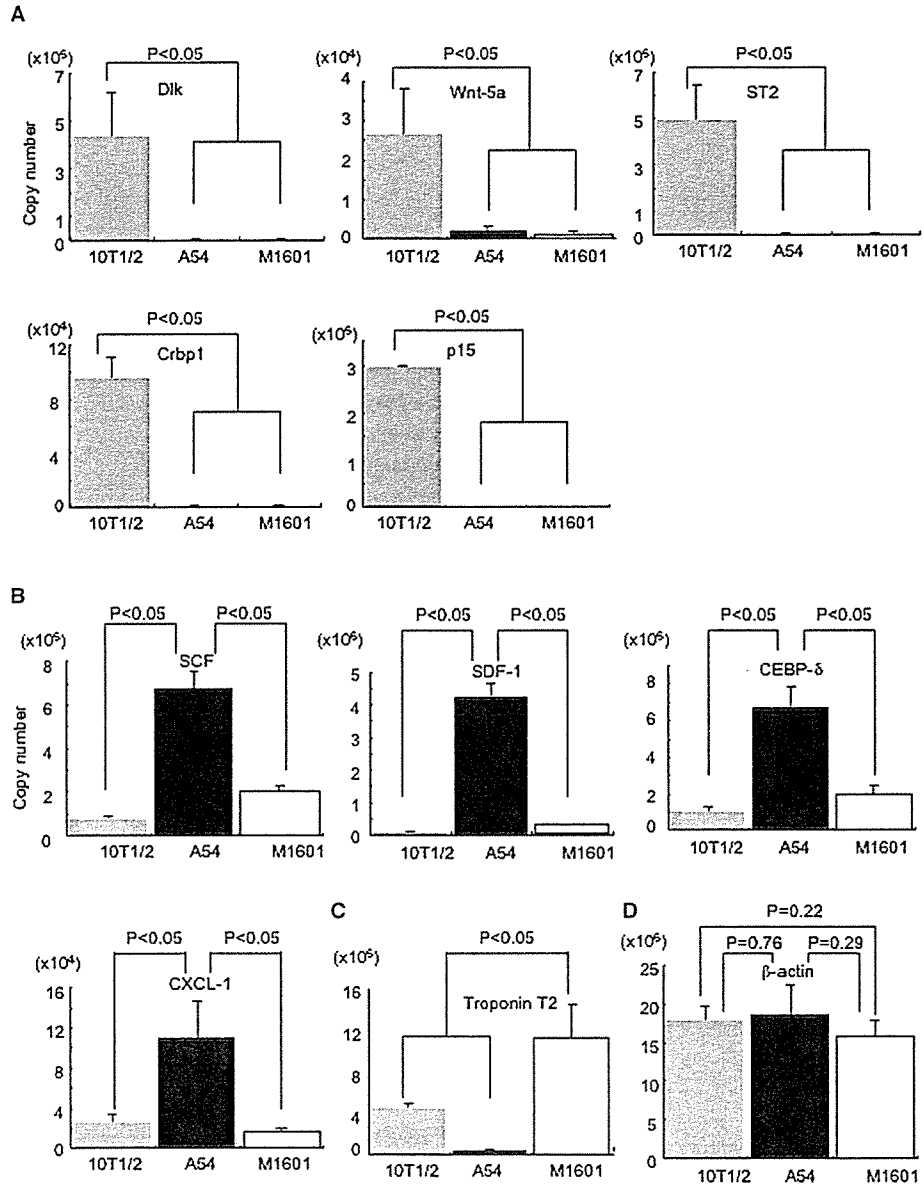

Figure 2. Up-regulated genes in 10T1/2(A), A54(B) and M1601(C) cells. Total RNA was extracted independently from the micro-array experiments and used to synthesize cDNA. The cDNA was subjected to real-time PCR with specific primers for Dlk, Wnt-5a, ST2, CrbpI and p15 (A), SCF, SDF-1 and adipogenic markers C/EBP-δ and CXCL-1 (B), cardiac troponin T2 (C) and β-actin (D). The copy number was used to compare the level of expression. The mean ± SD from three independent reactions using the same cDNA is shown.

we confirmed that the levels of transcripts for these genes were elevated in 10T1/2 cells. We also confirmed the up-regulation of CD90 in 10T1/2 cells by flow cytometry (data not shown). Although the function of CD90 in MSC is unclear, it may be useful for distinguishing immature MSC from committed progenitors because CD90 was not detected in the other two cell types. We analyzed the expression of the *Dlk* gene further, because *Dlk* is known to inhibit adipocyte and osteoblast differentiation [16]. Overexpression of human *Dlk* in A54 cells by transduction with a retroviral vector did not affect adipocyte differentiation (Figure 3). Further experiments are required to determine the function of the genes up-regulated in 10T1/2 cells.

SCF and SDF-1 are up-regulated in pre-adipocyte A54 cells

Previous studies have shown that pre-adipocytes have a greater ability to support hematopoiesis *in vitro* than other kinds of stromal cell components [24,25]. The results of

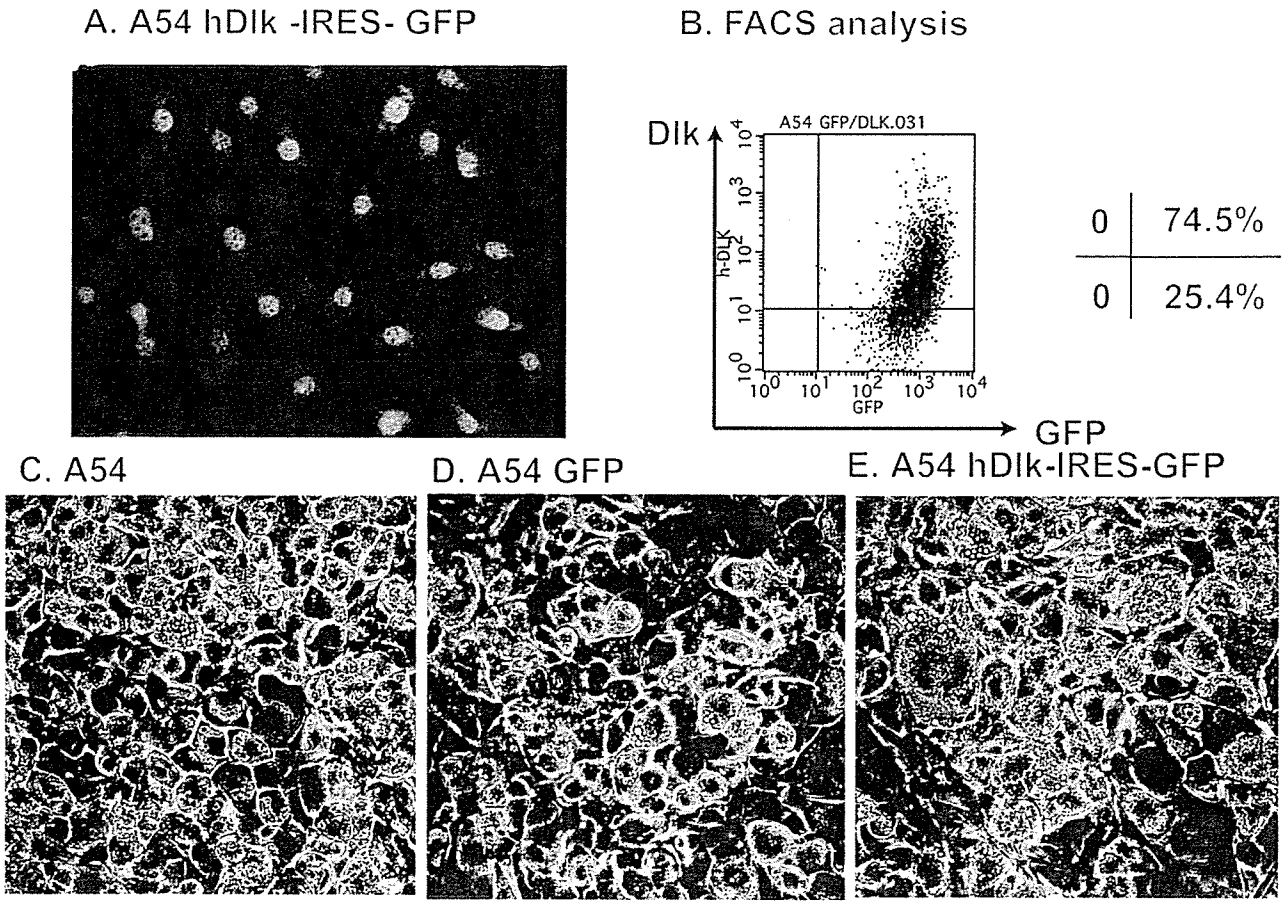

Figure 3. Enforced Dlk expression in A54 cells did not inhibit terminal differentiation into adipocyte. (A) GFP expression in A54 cells transfected with hDlk-IRES-EGFP. (B) Flow cytometric analysis for expression of hDlk in A54 cells transfected with hDlk-IRES-EGFP. (C–E) Adipocyte differentiation among parental A54 cells (C), A54 cells transfected with control IRES-EGFP (D) and A54 cells transfected with hDlk-IRES-EGFP (E).

our gene expression profiling revealed that critical cytokines for hematopoiesis, such as SCF and SDF-1, are upregulated in pre-adipocyte A54 cells. In addition, many chemokines, such as CXCL-1 and CCL-7, were also upregulated (Table 1B). We performed real-time PCR analysis of *SCF*, *SDF-1*, *CEBP-δ* and *CXCL-1*. As shown in Figure 2B, among the three cell lines the expression of these genes was highest in A54 cells. The level of Ang-1 mRNA in A54 cells was similar to that in OP9 cells (Figure 4A), which are a well-characterized BM stromal cell line. Moreover, of the three cell lines, A54 was the only one with which we could detect the expression of Ang-1 protein, and its level apparently decreased after adipocyte differentiation (Figure 4B).

The ability of the three cell lines to support formation of a cobblestone appearance

To examine the effects of these three lines on hematopoietic cells, we co-cultured them with a mouse hematopoietic stem cell fraction. The experimental protocol is shown in Figure 5A. The BM cells were depleted of lineage marker-positive cells using the Auto-MACS magnetic beads system. Thereafter Sca-1$^+$ cells were selected. The resulting Lin(−)Sca-1(+) fractions were plated on 10T1/2, A54, or M1601 cells in 12-well dishes. After 6 days of co-culture, a cobblestone appearance was observed only on the A54 cells (Figure 5B–D). These results suggest that, of the three cell lines, only A54 cells have the ability to support hematopoietic cell growth, which agrees with our previous report [12]. We did not observe hematopoietic cell colonies on the layer of the terminally differentiated A54 adipocytes (Figure 5E), suggesting that pre-adipocyte A54 cells lose the ability to support cobblestone formation after differentiation into adipocytes.

To understand the molecular mechanisms underlying this effect, we examined the levels of *SCF*, *SDF-1* and *Ang-1* expression after adipocyte differentiation by real-time

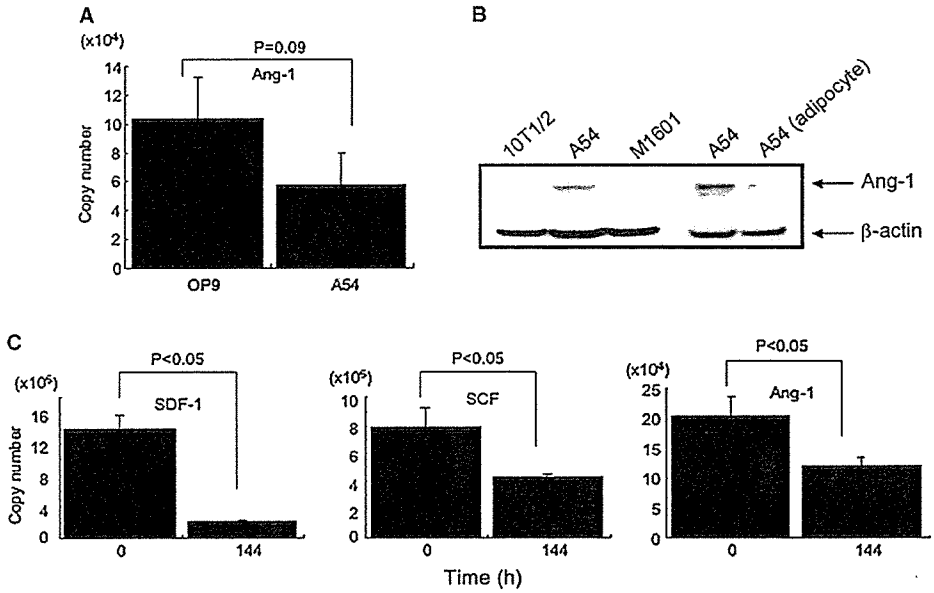

Figure 4. Ang-1 expression and down-regulation of SCF, SDF-1 and Ang-1 in A54 cells after adipocyte differentiation. (A) The level of Ang-1 mRNA in A54 cells was similar to that in OP9 cells, a well-characterized stromal cell line that supports the survival of hematopoietic stem cells. (B) Western blot analysis of Ang-1 protein expression among 10T1/2, A54, M1601 and A54 cells differentiated into adipocytes. (C) The changes in levels of SCF, SDF-1 and Ang-1 mRNA in A54 cells before and after adipocyte differentiation were monitored by real-time PCR. The copy number was used to compare the level of expression. The mean ± SD from three independent reactions using the same cDNA is

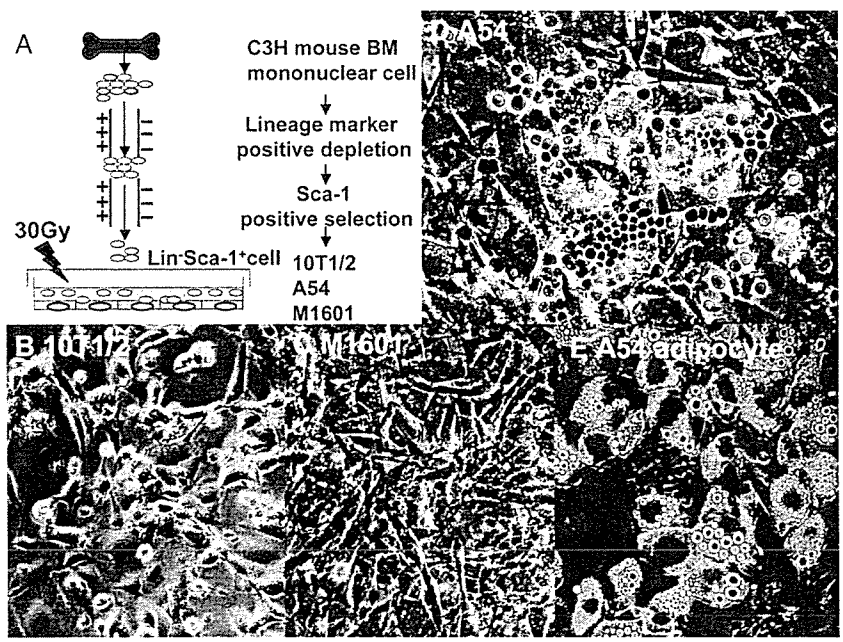

Figure 5. Formation of cobblestone appearance on 10T1/2, A54 and M1601 cells. (A) Experimental procedure. (B–E) 10T1/2, A54 and M1601 were co-cultured with a mouse hematopoietic stem cell fraction for 6 days. The formation of cobblestone appearance was evaluated by phase-contrast microscopy.

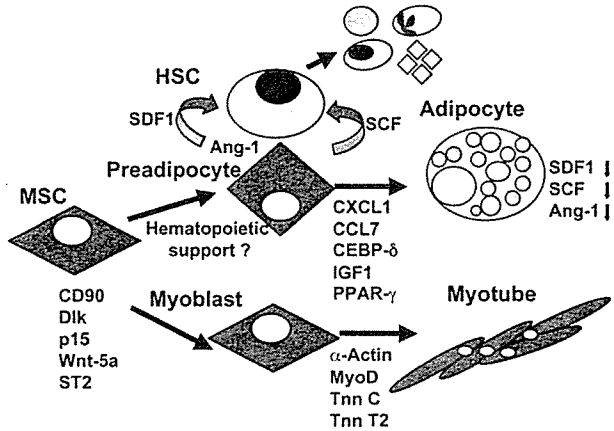

Figure 6. Proposed model for the hierarchy of the BM stromal system. Schematic relationship among MSC, pre-adipocytes and myoblasts and the up-regulated genes in each cell. The expression of CD90, Dlk, Wnt-5a and ST2 was up-regulated in 10T1/2 cells. The up-regulated genes in A54 (SCF, SDF-1, and Ang-1) were suppressed after adipocyte differentiation. The expression of α-actin, MyoD, troponin C and troponin T2 was up-regulated in M1601 cells.

PCR. As shown in Figure 4C, the expression of these genes decreased after the adipocyte differentiation.

Up-regulation of troponin T2 gene in M1601 cells

We confirmed that the expression of *cardiac troponin T2* was up-regulated in M1601 cells (Figure 2C). Figure 2D demonstrates that the level of β-actin expression in each line was almost the same.

Discussion

In the current studies, we used 10T1/2 and two 10T1/2-derived cell lines as models of MSC and progenitor cells. The genes regulating MSC differentiation remain obscure. Because primary MSC may contain heterogeneous progenitors and because the extent of differentiation may vary, it is difficult to use them for high-throughput analysis of gene expression. Therefore, we chose these three cell lines to avoid problems related to the heterogeneity of MSC; all three cell lines had the same genetic background because the A54 and M1601 cells were both derived from 10T1/2 cells.

Up-regulation of *Dlk* in 10T1/2 cells was confirmed by micro-array and RT real-time PCR. Although *Dlk* has been reported to inhibit adipocyte and osteoblast differentiation [16], overexpression of *Dlk* did not affect adipocyte differentiation of A54 cells. This is not surprising because other factor(s) may also be required for the inhibition of differentiation.

Wnt-5a is a member of the Wnt family, which plays an essential role in regulating proliferation and differentiation [19]. Our GeneChip analysis demonstrated that *Wnt-5a* was expressed in parental 10T1/2 cells and that the gene expression of its receptor, Frizzled, was up-regulated in the downstream progenitor cell line, A54. MSC may self-regulate their differentiation or proliferation in the BM through the Wnt-5a signaling system. The genes up-regulated in the parental 10T1/2 cells, namely, *Dlk*, *Wnt-5a*, *ST2*, *Crbpl*, *p15* and *CD90*, may be worth investigating further to identify molecules important for maintaining stemness.

SCF and *SDF-1* were exclusively up-regulated in A54 pre-adipocyte cells. This agreed with the ability of these cells to support hematopoietic cell growth. Adipocyte differentiation down-regulated the expression of these genes and reduced the ability of the A54 cells to support hematopoietic cell growth. These results indicate that pre-adipocytes may be one of the committed progenitors that participate in hematopoietic support and that the loss of this ability after terminal adipocyte differentiation may be involved in a fatty change of BM in aging or aplastic anemia. Ang-1 has been reported to be essential for the self-renewal of hematopoietic stem cells and to be expressed on osteoblasts in the BM niche [14]. Our results suggested that both pre-adipocytes and osteoblasts in the BM are Ang-1-producing cells. Pre-adipocytes appear to be related to osteoblasts because they express the mRNA for osteoblast-specific genes such as *osteocalcin* [26]. This suggests that there is a common molecular pathway in osteoblast and pre-adipocyte differentiation. Also, TAZ has been reported to be a key regulator of MSC differentiation. This protein enhances the differentiation of MSC into osteoblasts by activating Runx2 and suppresses the differentiation into adipocytes by inhibiting PPAR-γ [10].

We found that M1601 cells express *cardiac muscle-specific* gene, suggesting a possible plasticity of MSC to differentiate into cardiac muscle cells. In this study, we did not analyze the up-regulated genes in M1601 further. Human MSC differentiate into cardiac muscle cells *in vitro* upon treatment with 5-azacytidine and co-culture with primary mouse cardiac muscle cells [27]. A recent study demonstrated that allogenic MSC ameliorated cardiac function in pig myocardial infarction and rat dilated cardiomyopathy

models, suggesting that MSC have the potential to treat myocardial infarction and cardiomyopathy [28,29].

In Figure 6, we show our hypothesis of lineage- and stage-specific gene expression patterns in MSC and committed progenitors. The characterization of the transcriptional profiles should enhance the understanding of the molecular mechanisms underlying the differentiation of MSC into progenitors. Furthermore, we hypothesize that each progenitor has a unique function in BM. Our analysis has demonstrated a possible molecular mechanism of hematopoietic support by pre-adipocytes, and we found that pre-adipocyte progenitors may be better than MSC for hematopoietic engraftment in BM transplantation. Finally, because MSC contains heterogeneous progenitors and each committed progenitor has a different function in BM, the three cell lines analyzed here could be useful tools for characterizing the behavior and function of MSC.

References

1 Pittenger MF, Mackay AM, Beck SC. Multilineage potential of adult human mesenchymal stem cells. *Science* 1999;284:143–7.

2 Bensidhoum M, Chapel A, Francois S *et al.* Homing of *in vitro* expanded Stro-1$^-$ or Stro-1$^+$ human mesenchymal stem cells into the NOD/SCID mouse and their role in supporting human CD34 cell engraftment. *Blood* 2004;103:3313–9.

3 Maitra B, Szekely E, Gjini K *et al.* Human mesenchymal stem cells support unrelated donor hematopoietic stem cells and suppress T-cell activation. *Bone Marrow Transplant* 2004;33:597–604.

4 Zappia E, Casazza S, Pedemonte E *et al.* Mesenchymal stem cells ameliorate experimental autoimmune encephalomyelitis inducing T cell anergy. *Blood* 2005;106:1755–61.

5 Djouad F, Plence P, Bony C *et al.* Immunosuppressive effect of mesenchymal stem cells favors tumor growth in allogeneic animals. *Blood* 2003;102:3837–44.

6 Le Blanc K, Rasmusson I, Sundberg B *et al.* Treatment of severe acute graft-versus-host disease with third party haploidentical mesenchymal stem cells. *The Lancet* 2004;363:1439–41.

7 Lazarus HM, Koc ON, Devine SM *et al.* Cotransplantation of HLA-identical sibling culture-expanded mesenchymal stem cells and hematopoietic stem cells in hematologic malignancy patients. *Biol Blood Marrow Transplant* 2005;11:389–98.

8 Horwitz EM, Prockop DJ, Fitzpatrick LA *et al.* Transplantability and therapeutic effects of bone marrow-derived mesenchymal cells in children with osteogenesis imperfecta. *Nat Med* 1999;5:309–13.

9 Bang OY, Lee JS, Lee PH *et al.* Autologous mesenchymal stem cell transplantation in stroke patients. *Ann Neurol* 2005;57:874–82.

10 Hong JH, Hwang ES, McManus MT *et al.* TAZ, a transcriptional modulator of mesenchymal stem cell differentiation. *Science* 2005;309:1074–8.

11 Taylor SM, Jones PA. Multiple new phenotypes induced in 10T1/2 and 3T3 cells treated with 5-azacytidine. *Cell* 1979;17:771–9.

12 Nishikawa M, Ozawa K, Tojo A *et al.* Changes in hematopoiesis-supporting ability of C3H10T1/2 mouse embryo fibroblasts during differentiation. *Blood* 1993;81:1184–92.

13 Kopp HG, Avecilla ST, Hooper AT *et al.* Tie2 activation contributes to hemangiogenic regeneration after myelosuppression. *Blood* 2005;106:505–13.

14 Arai F, Hirao A, Ohmura M *et al.* Tie2/angiopoietin-1 signaling regulates hematopoietic stem cell quiescence in the bone marrow niche. *Cell* 2004;118:149–61.

15 Kume A, Xu R, Ueda Y *et al.* Long-term tracking of murine hematopoietic cells transduced with a bicistronic retrovirus containing CD24 and EGFP genes. *Gene Ther* 2000;14:1193–9.

16 Abdallah BM, Jensen CH, Gutierrez G *et al.* Regulation of human skeletal stem cells differentiation by Dlk1/Pref-1. *J Bone Miner Res* 2004;19:841–52.

17 Sakamoto K, Yamaguchi S, Ando R *et al.* The nephroblastoma overexpressed gene (NOV/ccn3) protein associates with Notch1 extracellular domain and inhibits myoblast differentiation via Notch signaling pathway. *J Biol Chem* 2002;277:29399–405.

18 Schoonjans K, Staels B, Auwerx J. The peroxisome proliferator activated receptors (PPARS) and their effects on lipid metabolism and adipocyte differentiation. *Biochim Biophys Acta* 1996;130:93–109.

19 Bennett CN, Ross SE, Longo KA *et al.* Regulation of Wnt signaling during adipogenesis. *J Biol Chem* 2002;277:30998–1004.

20 Lijnen HR, Alessi MC, Van Hoef B *et al.* On the role of plasminogen activator inhibitor-1 in adipose tissue development and insulin resistance in mice. *J Thromb Haemost* 2005;3:1174–9.

21 Kumar S, Leontovich A, Coenen MJ *et al.* Gene expression profiling of orbital adipose tissue from patients with Graves' ophthalmopathy: a potential role for secreted frizzled-related protein-1 in orbital adipogenesis. *J Clin Endocrinol Metab* 2005;90:4730–5.

22 Lassar AB, Buskin JN, Lockshon D *et al.* MyoD is a sequence-specific DNA binding protein requiring a region of myc homology to bind to the muscle creatine kinase enhancer. *Cell* 1989;58:823–31.

23 Cooper TA, Ordahl CP. A single troponin T gene regulated by different programs in cardiac and skeletal muscle development. *Science* 1984;226:979–82.

24 Maekawa TL, Takahashi TA, Fujihara M *et al.* A novel gene (drad-1) expressed in hematopoiesis-supporting stromal cell lines, ST2, PA6 and A54 preadipocytes: use of mRNA differential display. *Stem Cells* 1997;15:334–9.

25 Mazini L, Wunder E, Sovalat H *et al.* Mature accessory cells influence long-term growth of human hematopoietic progenitors on a murine stromal cell feeder layer. *Stem Cells* 1998;16:404–12.

26 Dorheim MA, Sullivan M, Dandapani V *et al*. Osteoblastic gene expression during adipogenesis in hematopoietic supporting murine bone marrow stromal cells. *J Cell Physiol* 1993;154:317–28.

27 Shim WS, Jiang S, Wong P *et al*. Ex vivo differentiation of human adult bone marrow stem cells into cardiomyocyte-like cells. *Biochem Biophys Res Commun* 2004;324:481–8.

28 Amado LC, Saliaris AP, Schuleri KH *et al*. Cardiac repair with intramyocardial injection of allogeneic mesenchymal stem cells after myocardial infarction. *Proc Natl Acad Sci USA* 2005;102:11474–9.

29 Nagaya N, Kangawa K, Itoh T *et al*. Transplantation of mesenchymal stem cells improves cardiac function in a rat model of dilated cardiomyopathy. *Circulation* 2005;112:1128–35.

30 Nakano T, Kodama H, Honjo T. *In vitro* development of primitive and definitive erythrocytes from different precursors. *Science* 1996;272:722–4.

Available online at www.sciencedirect.com
ScienceDirect
Biochemical and Biophysical Research Communications 355 (2007) 956–962
BBRC
www.elsevier.com/locate/ybbrc

Interferon-γ and NF-κB mediate nitric oxide production by mesenchymal stromal cells

I. Oh, K. Ozaki *, K. Sato, A. Meguro, R. Tatara, K. Hatanaka, T. Nagai, K. Muroi, K. Ozawa *

Division of Hematology, Jichi Medical University, 3311-1 Yakushiji, Shimotsuke-shi, Tochigi 329-0498, Japan

Received 31 January 2007
Available online 21 February 2007

Abstract

Mesenchymal stromal cells (MSCs) have been shown to have an immunosuppressive effect. Previously, we demonstrated that nitric oxide (NO) is one of the immunomodulatory mediators of MSCs. We herein show that primary mouse bone marrow MSCs and three cell lines that mimic MSCs suppress both differentiation and proliferation in Th1 condition, whereas the suppression in Th2 condition is mild. NO production is inversely correlated with T cell proliferation in Th1 and Th2 conditions. NO is highly induced in Th1 and minimally induced in Th2. Moreover, an inhibitor of NO synthase restores both proliferation and interferon-γ (IFN-γ) production in Th1 condition. Furthermore, an anti-IFN-γ antibody strongly inhibits NO production and an inhibitor of NF-κB reduces the level of induction of inducible NO synthase (iNOS) in MSCs. Taken together, our results suggest that NO plays a significant role in the modification of Th1 and Th2 differentiation by MSCs, and that both IFN-γ and NF-κB are critical for NO production by MSCs.

Keywords: Mesenchymal stem cells; Nitric oxide production; Interferon-γ; NF-κB; Th1 differentiation; Th2 differentiation; Immunosuppression; 10T1/2; iNOS

Although many reports indicate that mesenchymal stromal cells (MSCs) suppress T cell proliferation, the molecular mechanisms involved are poorly understood [1–6]. Human MSCs were reported to suppress Th1 differentiation and augment Th2 differentiation [4]. In this study, we investigated whether mouse bone-marrow-derived MSCs have the same effect on Th1 and Th2 differentiation while were also trying to identify the underlying molecular mechanisms of these effects.

Naïve helper T cells primarily differentiate into either Th1 or Th2 cells. Th1 cells produce IFN-γ and interleukin-2 (IL-2) while Th2 cells produce IL-4, IL-5, and IL-13. In addition, it appears that a disruption of the balance between Th1 and Th2 differentiation is associated with the development of immune diseases [7,8].

Previously, two sub-lines of the parental C3H10T1/2 (10T1/2) cell line were established by treatment of that line with 5-azacytidine. These were characterized as a preadipocyte cell line and a myoblast cell line, and were designated A54 and M1601, respectively [9]. A54 and M1601 differentiate into adipocyte and myotube under defined conditions [9]. Other studies suggest that 10T1/2 cells have the same T cell suppressive effect as primary MSCs [10]. In addition, the 10T1/2 cell line has been used as a model of MSCs [11–14]. In the present study, these three cell lines were used as MSC-like cells and demonstrated that their phenotype is similar to that of primary MSCs.

Nitric oxide (NO) is known to suppress T cell proliferation [15–18]. Previously, we demonstrated that NO is one of the major mediators of T cell suppression by mouse MSCs [19]. It is possible that NO also plays a critical role

* Corresponding authors. Fax: +81 285 44 5258.
E-mail addresses: ozakikat@jichi.ac.jp (K. Ozaki), kozawa@ms2.jichi.ac.jp (K. Ozawa).

0006-291X/$ - see front matter © 2007 Elsevier Inc. All rights reserved.
doi:10.1016/j.bbrc.2007.02.054

in Th1/Th2 differentiation and the present study demonstrates that NO contributes to preferential Th1 suppression by MSCs. Moreover, the results indicate that IFN-γ and NF-κB are key regulators of NO production by MSCs.

Materials and methods

Reagents. Anti-mouse CD3/CD28 beads (Dynal Biotech., Oslo, Norway) were used at 10 μl per 10^6 cells. PE-anti-IFN-γ and PE-anti-IL-4 antibodies (BD Biosciences, San Diego, CA) were used for intracellular staining of cytokines. Murine IL-4 and IL-12 were purchased from R&D Systems (Minneapolis, MN). The neutralizing antibodies for IFN-γ and IL-4 were purchased from BD Biosciences.

NG-monomethyl-L-arginine (L-NMMA) was from Wako Pure Chemical Industries (Osaka, Japan). Lipopolysaccharide (LPS) was purchased from Sigma–Aldrich (St. Louis, MO). Tumor necrosis factor-α (TNF-α), IL-1β, soluble TNF-α receptor, and neutralizing anti-IL-1β antibody were purchased from PeproTech (Rocky Hill, NJ). CpG oligonucleotide (HyCult biotechnology, Netherlands), poly(I:C), and flagellin (InvivoGen, San Diego, CA) were generous gifts from Dr. Motoharu Matsuura (Jichi Medical University). NF-κB inhibitor, Bay-11-7085 [20] was purchased from Wako.

Primary MSCs and MSC-like cell lines. The C3H10T1/2 cell line was obtained from ATCC (American Type Culture Collection). The A54 (preadipocyte) and M1601 (myoblast) cell lines were 10T1/2-derived cell lines [9]. Primary MSCs were generated, maintained, and characterized as previously described [19].

Intracellular staining. Cytofix/Cytoperm® (BD Biosciences) was used for fixation/permeabilization. Then, cells were stained with anti-IFN-γ or anti-IL-4 antibody (BD Biosciences).

Th1 and Th2 differentiation. Splenic $CD4^+$ T cells were selected using the autoMACS magnetic beads system (Milteny Biotech., Auburn, CA) and stimulated with anti-mouse CD3/CD28 beads (Dynal Biotech.) at an appropriate concentration for 2–3 days with or without MSCs. The purity of the cells, determined by flow cytometry using antibodies against CD4 and B220, was approximately 90%. Stimulation was performed under Th1 (10 ng/ml IL-12 and 10 μg/ml anti-IL-4) or Th2 (100 ng/ml IL-4 and 10 μg/ml anti-IFN-γ) polarizing conditions. For intracellular staining, after extensive washing, Golgistop® (Monensin, 2 μM, BD Biosciences) was added, and then the cells were re-stimulated with PMA and ionomycin for 6 h. For enzyme-linked immunosorbent assay (ELISA), after extensive washing, cells were incubated overnight with plate-bound anti-CD3 antibody and the supernatants were subjected to quantification of IFN-γ or IL-4.

Carboxyfluorescein succinimidyl ester (CFSE) labeling. $CD4^+$ T cells were resuspended at a concentration of 1×10^7 cells/ml in PBS. CFSE (Invitrogen) was added to a final concentration of 10 μM and incubated 10 min at 37 °C. Labeling was stopped by washing with RPMI plus 10% fetal calf serum (FCS). Cells were stimulated with anti-CD3/CD28 beads in the presence or absence of MSCs for 3 days. In some experiments 1 mM of L-NMMA, an inhibitor of NO synthase, was added to the culture.

IFN-γ or IL-4 concentration. Commercially available ELISA kits were used for the quantification of IFN-γ or IL-4 in supernatants after Th1 and Th2 differentiation, according to the manufacturer's instruction (BD Biosciences).

Measurement of NO production. The concentration of NO in cell culture supernatants was determined by using a Griess reagent kit (Wako Pure Chemical Industries) according to the manufacturer's instructions.

Flow cytometric analysis. Cells were incubated with Fc block® (BD Biosciences) to inhibit non-specific binding of antibodies to Fc receptors.

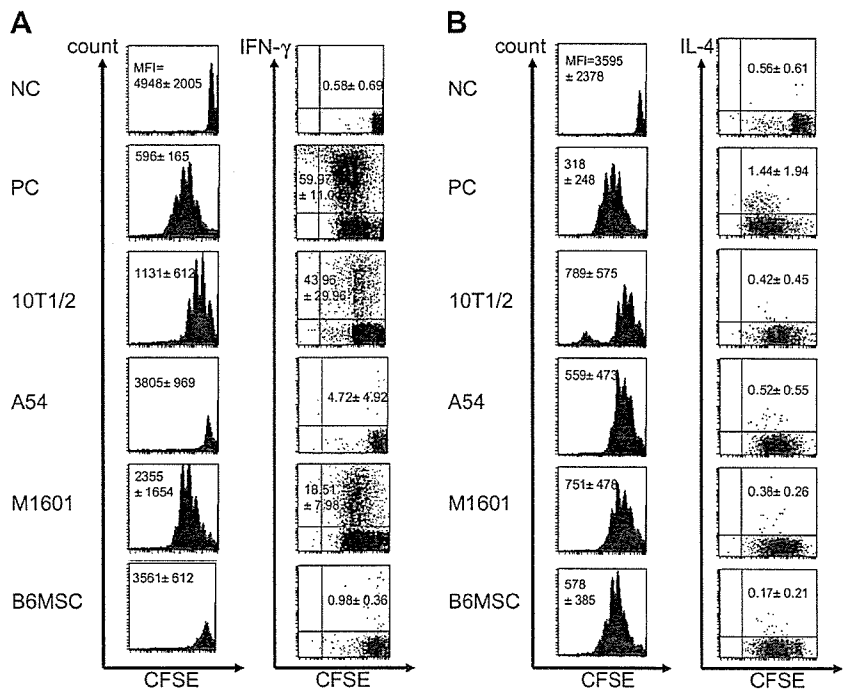

Fig. 1. Th1 and Th2 differentiation in the presence of MSCs. (A) A simultaneous flow cytometric analysis of T cell differentiation and proliferation in Th1 condition. Splenic $CD4^+$ T cells were selected with autoMACS , stained with CFSE, and stimulated in Th1 condition for 72 h. To prevent cytokine secretion, monensin (2 μM) was added during the last 6 h. Then, cells were extensively washed and intracellular-stained with anti-IFN-γ antibody (right panel). The divided cells show a lower intensity of CFSE staining (left panel). (B) A simultaneous flow cytometric analysis of T cell differentiation and proliferation in Th2 condition. Cell preparation was the same as (A) but cells were stimulated in Th2 condition and stained with anti-IL-4 antibody. The numbers indicated in left panels are mean ± SD of mean fluorescein intensity and that in right panels are mean ± SD of the percentage of cells in upper right quadrant. The small isolated CFSE-negative-peak in 10T1/2 in (B) was detached 10T1/2 cells during the washing step. NC, negative control; $CD4^+$ T cells alone; PC, positive control; $CD4^+$ T cells with mitogen and without MSCs.

Then, cells were stained in FACS buffer (PBS supplemented with 10% FBS) with appropriate concentrations of antibodies for 30 min on ice, washed with FACS buffer, and analyzed with a BD LSR cytometer (BD Biosciences), and the data were analyzed using CELLQUEST software (BD Biosciences).

[^{3}H]Thymidine incorporation, immunoblot analysis, detection of inducible NO synthase (iNOS) expression. We performed these assays as described previously [19].

Results

Effects of MSCs on Th1 differentiation

Using primary MSCs and three MSC-like cell lines, the effects of co-cultivation of MSCs on Th1 and Th2 differentiation were examined. Fig. 1A, left panel illustrates that primary MSCs and the A54 cell line strongly suppressed proliferation in Th1 condition. The 10T1/2 and M1601 cells also showed modest suppression. Consistent with this, [^{3}H]thymidine incorporation demonstrated strong suppression of T cell proliferation in the presence of primary MSCs and the A54 cell line and modest suppression in the presence of the 10T1/2 and M1601 cell lines (Supplementary Fig. 1A).

Simultaneously, the production of IFN-γ in the presence of MSCs was examined. In addition to the suppression of T cell proliferation, IFN-γ production is also strongly suppressed in the presence of primary MSCs and the A54 cell line (Fig. 1A, right panel). This suppression was not due to the suppressed number of T cells because the suppression of IFN-γ was also observed with an ELISA, in which an equal number of differentiated cells were used (Supplementary Fig. 1C).

Effects of MSCs on Th2 differentiation

In contrast to Th1 differentiation, a modest suppression of Th2 cell proliferation was observed by a flow cytometric analysis (Fig. 1B, left panel). Specifically, primary MSCs and the A54 cell line showed significantly less suppression compared to the suppression in Th1 condition (Fig. 1B, left panel vs. Fig. 1A, left panel). Consistent with this, [^{3}H]thymidine incorporation assay demonstrated a less suppression of T cell proliferation in Th2 as compared to Th1 in the presence of primary MSCs and A54 cell line (Supplementary Fig. 1B vs. 1A). IL-4 production in the presence of MSCs was suppressed in Th2 condition, as measured by both flow cytometric analysis (Fig. 1B, right panel) and ELISA, in which the same number of differentiated cells were used (Supplementary Fig. 1D).

Nitric oxide production in Th1/Th2 differentiation

Since nitric oxide (NO) is one of the primary mediators of T cell suppression by MSCs [19], it is possible that NO is also involved in suppression of proliferation in Th1 condition. We found a reverse correlation between NO production and T cell proliferation in Th1/Th2 conditions (Fig. 2A and B), where NO production was highly induced in the presence of MSCs in Th1 but it was induced only minimally in Th2. In particular, primary MSCs and the A54 preadipocyte cell line, which induce strong T cell suppression in Th1 (Fig. 1A), produce high levels of NO in Th1 condition (Fig. 2A). These results suggest that NO also plays a major role in the preferential suppression of Th1 proliferation by MSCs.

Inhibition of NO synthase restores proliferation and differentiation of Th1 cells

To confirm the role of NO, a specific NO synthase inhibitor, NG-monomethyl-L-arginine (L-NMMA) was used. The presence of this inhibitor restored the T cell proliferation and IFN-γ production in Th1 condition (Fig. 3A and B), demonstrating that NO is a mediator of suppression of both T cell growth and IFN-γ production in Th1 condition. However, L-NMMA does not completely restore the T cell proliferation by primary MSCs, suggesting that there are other factors involving in this suppression, as demonstrated in the previous study [19].

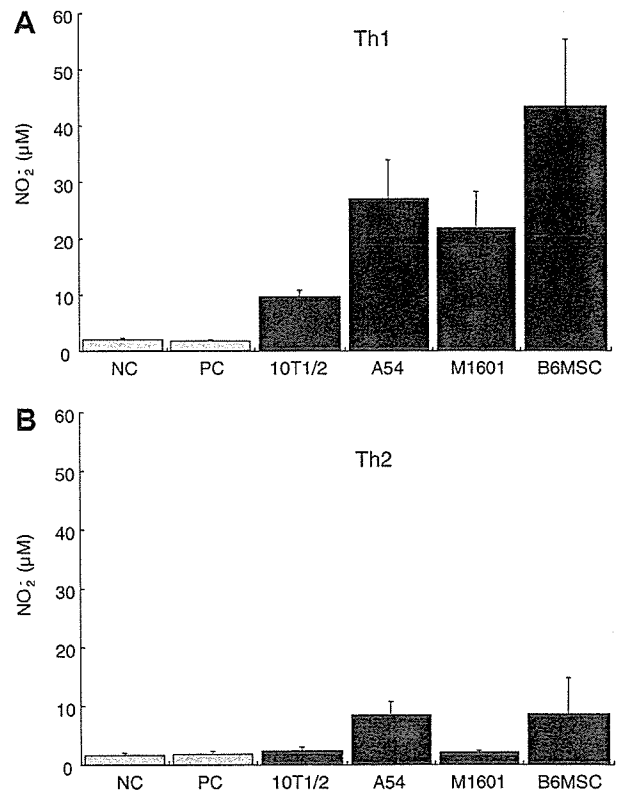

Fig. 2. NO production in Th1 and Th2 conditions in the presence of MSCs. (A) NO production in Th1 condition in the presence of MSCs. (B) NO production in Th2 condition in the presence of MSCs. Splenic $CD4^+$ T cells (1×10^6) were stimulated in either Th1 or Th2 condition in the presence of 10T1/2, A54, M1601, and primary MSCs (1×10^5) for 48 h. The concentration of NO_2 in supernatants were determined by the Greiss assay. NC, negative control; $CD4^+$ T cells alone; PC, positive control; $CD4^+$ T cells with mitogen and without MSCs.